

LATTICE BOLTZMANN APPROACH TO VISCOUS FLOWS BETWEEN PARALLEL PLATES

BÉLA SZILÁGYI

Department of Theoretical and Computational Physics
University of Timișoara
Bd. Vasile Pârvan 4, RO – 1900 Timișoara, Romania

ROMEO SUSAN – RESIGA

Department of Hydraulic Machinery, Technical University of Timișoara
Bd. Mihai Viteazul 1, RO – 1900 Timișoara, Romania

VICTOR SOFONEA

Research Center for Hydrodynamics, Cavitation and Magnetic Fluids
Technical University of Timișoara
Bd. Mihai Viteazul 1, RO – 1900 Timișoara, Romania

Abstract

Four different kinds of laminar flows between two parallel plates are investigated using the Lattice Boltzmann Method (LBM). The LBM accuracy is estimated in two cases using numerical fits of the parabolic velocity profiles and the kinetic energy decay curves, respectively. The error relative to the analytical kinematic viscosity values was found to be less than one percent in both cases. The LBM results for the unsteady development of the flow when one plate is brought suddenly at a constant velocity, are found in excellent agreement with the analytical solution. Because the classical Schlichting's approximate solution for the entrance-region flow is not valid for small Reynolds numbers, a Finite Element Method solution was used in order to check the accuracy of the LBM results in this case.

keywords: laminar flow, parallel plates, velocity profile, Lattice Boltzmann.

1 Introduction

Since Frisch, Hasslacher and Pomeau [1, 2], have shown that particles moving on a hexagonal lattice with very simple collisions rules on its nodes lead to the Navier-Stokes equation, the use of lattice gas models (LGM) to study hydrodynamics has received considerable interest.

The Lattice Boltzmann Method (LBM) [3, 4, 5], a derivative of the lattice gas automaton method, uses real numbers instead of bits to represent particle distributions, being far less noisy than LGM. The LBM is a finite-difference technique for solving the kinetic equation in discrete space and discrete time; the Navier-Stokes equation is recovered in the long-wavelength and low-frequency limit.

This paper presents a LBM study of four different laminar flows between two parallel plates. Both steady and unsteady flows are simulated; the numerical results are compared with analytical solutions or Finite Element Method (FEM) results.

2 Lattice Boltzmann Method and Single Time Relaxation Approximation

In the LBM, the evolution equation for the particle distribution functions $n_i(\vec{x}, t)$ corresponding to the velocities \vec{c}_i , $i = 0, 1, \dots, 6$ ($\vec{c}_0 = \vec{0}$, $|\vec{c}_j| = 1$, $j = 1, 2, \dots, 6$) defined on a two dimensional hexagonal lattice [5] can be written as follows:

$$n_i(\vec{x} + \vec{c}_i, t + 1) = n_i(\vec{x}, t) + \Omega(n_i(\vec{x}, t)) \quad (1)$$

where $\Omega_i = \Omega(n_i(\vec{x}, t))$ is the local collision operator, depending only on the local particle distribution functions n_i .

Chen et al. [5] used the single time relaxation approximation

$$\Omega_i = -\frac{n_i - n_i^{eq}}{\tau} \quad (2)$$

where the equilibrium distribution function n_i^{eq} depends upon the local fluid variables and the lattice relaxation time τ controls the evolution to the equilibrium state.

The total mass n and local momentum $n\vec{u}$ are conserved after collisions:

$$n = \sum_i n_i = \sum_i n_i^{eq} \quad (3)$$

$$n\vec{u} = \sum_i \vec{c}_i n_i = \sum_i \vec{c}_i n_i^{eq} \quad (4)$$

The volumic density ρ for a hexagonal lattice is expressed in terms of n [6]:

$$\rho = \frac{n}{\sqrt{3}/2} \quad (5)$$

To derive the mass and momentum conservation equations, a Taylor expansion in time and space of eq.(1) is performed in the long-wavelength and low-

frequency limit. Using the Chapman-Enskog procedure, the final results are:

$$\frac{\partial n}{\partial t} + \frac{\partial}{\partial x_\alpha}(nu_\alpha) = 0 \quad (6)$$

$$\frac{\partial(nu_\alpha)}{\partial t} + \frac{\partial}{\partial x_\beta} \left[\sum_i c_{i\alpha} c_{i\beta} n_i^{eq} - \frac{2\tau-1}{2} \frac{\partial}{\partial x_\gamma} \sum_i c_{i\alpha} c_{i\beta} c_{i\gamma} n_i^{eq} \right] = 0 \quad (7)$$

For the hexagonal lattice we have:

$$\vec{c}_i = (c_{i1}, c_{i2}) = \left(\cos \frac{\pi(i-1)}{3}, \sin \frac{\pi(i-1)}{3} \right) \quad i = 1, 2 \dots 6 \quad (8)$$

$$n_i^{eq} = n \left[\frac{1-d_0}{6} + \frac{1}{3}(\vec{c}_i \cdot \vec{u}) + \frac{2}{3}(\vec{c}_i \cdot \vec{u})^2 - \frac{u^2}{6} \right] \quad i = 1, 2 \dots 6 \quad (9)$$

$$n_0^{eq} = n [d_0 - u^2] \quad (10)$$

where $d_0 \in (0, 1)$ is a constant. This leads to:

$$\sum_i c_{i\alpha} c_{i\beta} n_i^{eq} = \frac{n(1-d_0)}{2} \quad (11)$$

$$\frac{\partial}{\partial x_\gamma} \sum_i c_{i\alpha} c_{i\beta} c_{i\gamma} n_i^{eq} = \frac{1}{2} S_{\alpha\beta} + \frac{1}{4} n (\nabla \cdot \vec{u}) \delta_{\alpha\beta} \quad (12)$$

where $S_{\alpha\beta} = \frac{1}{2} \left(\frac{\partial u_\beta}{\partial x_\alpha} + \frac{\partial u_\alpha}{\partial x_\beta} \right)$ is the time-rate-of-strain tensor.

Dividing (7) with $\sqrt{3}/2$ and identifying the pressure as $p = \rho(1-d_0)/2$, the Navier-Stokes equation in the incompressible limit ($\nabla \cdot \vec{u} = 0$) is obtained as:

$$\frac{\partial(\rho\vec{u})}{\partial t} + \nabla \cdot \left(p\vec{I} + \rho\vec{u}\vec{u} - \frac{2\tau-1}{4} \rho\vec{S} \right) = 0 \quad (13)$$

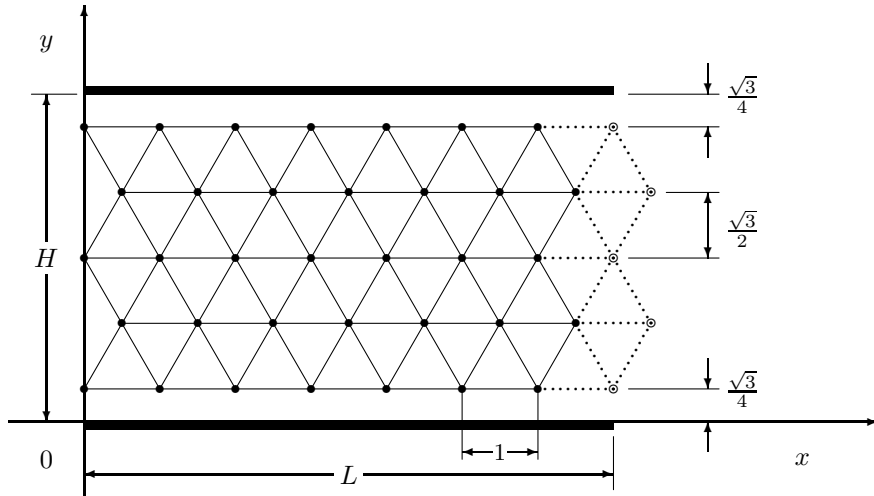
from which we can identify the shear η and kinematic ν viscosities:

$$\eta = \rho \frac{2\tau-1}{8} \quad \text{and} \quad \nu = \frac{2\tau-1}{8} \quad (14)$$

At the beginning of each run, the fluid was always considered to be at rest ($\vec{u} = 0$). By choosing $\rho = 2.1/(\sqrt{3}/2)$ and $d_0 = 1/7$, we have an uniform particle distribution $n_i = 0.3, i = 0, 1, 2 \dots 6$ at each node. For each time step, the following successive operations are performed at every lattice node:

- the local velocity is computed from (4);
- the equilibrium distribution functions $n_i^{eq}(\vec{x}, t)$ are computed from (9) and (10);
- using (1) and (2), the propagation step is performed in order to obtain the $n_i(\vec{x} + \vec{c}_i, t+1)$ distributions;
- if a body force exist, the new n_i distributions are modified according to the induced particle momentum change during one time step.

Figure 1: The flow domain and the hexagonal lattice



3 Flow between parallel rest plates

Fig 1. shows the flow domain between two parallel plates and the hexagonal two-dimensional lattice. The lattice is periodic in the flow direction, therefore the right nodes, connected with broken lines, coincide with the left ones. If N_l is the number of nodes along the x direction, the domain length is $L = N_l$ because the unit length is the triangle side. The distance between two node rows in the y direction is $\sqrt{3}/2$. Because of the "bounce-back" rules imposed in order to satisfy the no-slip conditions on both planes [7], the zero-velocity boundaries are located at a distance $\sqrt{3}/4$ from the lowest and highest rows. If we denote with N_w the number of node rows in the y direction, the distance between the two real plates is $H = N_w \sqrt{3}/2$.

3.1 Steady unidirectional flow

If the local velocity vector has the same direction everywhere and is independent of distance in the flow direction, the convective rate of change of velocity will vanish and the acceleration of a fluid element will be $\partial \vec{u} / \partial t$, with only one non-zero component. In addition, if we consider a steady flow, even this acceleration component will be zero.

The motion between two rest parallel plates can survive the viscous dissipation of energy only if there is a continuous energy supply to the fluid by a pressure gradient ∇p , which must be also independent of x . When ∇p is negative, the pressure gradient represents an uniform body force per unit volume $\rho \vec{f}$ in the direction of the positive x -axis [8].

The x component of the equation of motion reduces to:

$$f + \nu \frac{\partial^2 u}{\partial y^2} = 0 \quad (15)$$

The solution which satisfies the boundary conditions $u(0) = 0$ and $u(H) = 0$ is:

$$u(y) = \frac{f}{\nu} \frac{H^2}{2} \left(\frac{y}{H} - \frac{y^2}{H^2} \right) \quad (16)$$

with the maximum value

$$u_{max} = 0.125 \frac{f H^2}{\nu} \quad (17)$$

Both the equations (15) and (17) can be used in order to make a comparison between analytical (eq.14) and numerical results. As an example, the kinematic viscosity ν can be calculated by using the second derivative of $u(y)$ from (15) or the maximum velocity u_{max} from (17). The first possibility was preferred in this paper because it takes into account the whole velocity profile shape. If we use the least square method to fit a parabola between (y_i, u_i) points, $i = 1 \dots N_w$, we will have for the second derivative

$$\frac{\partial^2 u}{\partial y^2} = -2 \frac{\sum_i u_i (y_i H - y_i^2)}{\sum_i (y_i H - y_i^2)^2} \quad (18)$$

The body force per unit volume, $\rho \vec{f}$, must equalize the decay of the momentum ρu during one time step

$$\rho f = \frac{\partial(\rho u)}{\partial t} \quad (19)$$

Taking into account that $\delta t = 1$ for LBM, and

$$\delta(\rho u) = \frac{2 \delta n}{\sqrt{3}/2} \quad (20)$$

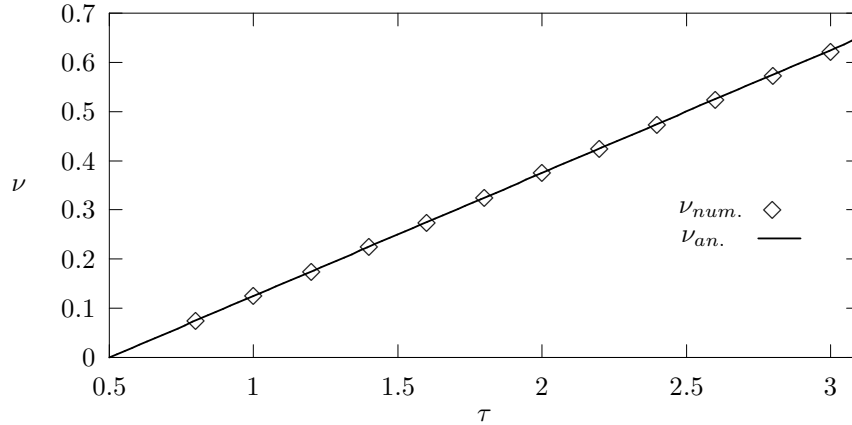
where δn is the value to be added to n_1 , respectively subtracted from n_4 at each step, according with (5) we obtain:

$$f = \frac{2\delta n}{n} \quad (21)$$

Finally, from (15),(18) and (21) the kinematic viscosity is:

$$\nu = \frac{\delta n}{n} \frac{\sum_i (y_i H - y_i^2)^2}{\sum_i u_i (y_i H - y_i^2)} \quad (22)$$

Figure 2: Numerical values for the kinematic viscosity ν , obtained by fitting the parabolic profiles for $0.8 \leq \tau \leq 3$; the solid line corresponds to the analytical formula (14).



The numerical results were obtained using a lattice with $N_l = 100$, $N_w = 101$ ($H = 87.4686$). For $\tau \geq 0.8$ we considered $\delta n = 10^{-6}$, and the numerical values for ν are represented in Fig. 2, together with the analytical line (14). The relative error does not exceed 0.8%.

A special attention was given for $0.5 < \tau < 0.8$, the results being presented in Table 1. It should be noticed that δn must be decreased when τ , respectively ν , diminish in order to have only positive n_i values, for each node and direction.

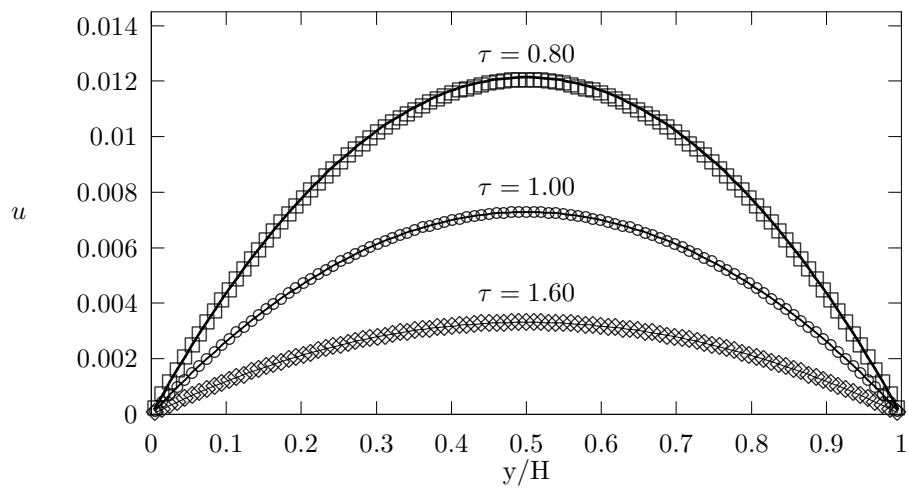
Table 1 also shows the number of steps needed to reach the steady state and the corresponding maximum velocity u_{max} (see eq.17). The relative difference between theoretical and analytical values, $\varepsilon_\nu = |\nu_{an} - \nu_{num}|/\nu_{an}$, does not exceed one percent.

Three velocity profiles are represented in Fig.3. A very good agreement exist between the theoretical parabola (solid curve) and the numerical results.

Table 1: Kinematic viscosities (ν_{an} from (14) and ν_{num} obtained by fitting parabolic velocity profiles) for $0.5 < \tau \leq 0.8$.

τ	δn	steps	u_{max}	ν_{an}	ν_{num}	ε_ν [%]
0.51	10^{-15}	$2.0 \cdot 10^6$	$3.6 \cdot 10^{-10}$	$2.50 \cdot 10^{-3}$	$2.5074 \cdot 10^{-3}$	0.29
0.52	10^{-14}	$8.0 \cdot 10^5$	$1.8 \cdot 10^{-9}$	$5.00 \cdot 10^{-3}$	$5.0353 \cdot 10^{-3}$	0.71
0.53	10^{-13}	$6.0 \cdot 10^5$	$1.2 \cdot 10^{-8}$	$7.50 \cdot 10^{-3}$	$7.5255 \cdot 10^{-3}$	0.34
0.54	10^{-12}	$4.0 \cdot 10^5$	$9.1 \cdot 10^{-8}$	$1.00 \cdot 10^{-2}$	$1.0059 \cdot 10^{-2}$	0.59
0.55	10^{-12}	$3.5 \cdot 10^5$	$7.3 \cdot 10^{-8}$	$1.25 \cdot 10^{-2}$	$1.2546 \cdot 10^{-2}$	0.37
0.56	10^{-11}	$3.5 \cdot 10^5$	$6.1 \cdot 10^{-7}$	$1.50 \cdot 10^{-2}$	$1.5019 \cdot 10^{-2}$	0.13
0.57	10^{-11}	$3.0 \cdot 10^5$	$5.2 \cdot 10^{-7}$	$1.75 \cdot 10^{-2}$	$1.7522 \cdot 10^{-2}$	0.13
0.58	10^{-11}	$3.0 \cdot 10^5$	$4.6 \cdot 10^{-7}$	$2.00 \cdot 10^{-2}$	$2.0011 \cdot 10^{-2}$	0.06
0.59	10^{-10}	$3.0 \cdot 10^5$	$4.0 \cdot 10^{-6}$	$2.25 \cdot 10^{-2}$	$2.2506 \cdot 10^{-2}$	0.03
0.60	10^{-10}	$3.0 \cdot 10^5$	$3.6 \cdot 10^{-6}$	$2.50 \cdot 10^{-2}$	$2.5004 \cdot 10^{-2}$	0.02
0.62	10^{-9}	$2.5 \cdot 10^5$	$3.0 \cdot 10^{-5}$	$3.00 \cdot 10^{-2}$	$3.0005 \cdot 10^{-2}$	0.02
0.64	10^{-9}	$2.0 \cdot 10^5$	$2.6 \cdot 10^{-5}$	$3.50 \cdot 10^{-2}$	$3.5008 \cdot 10^{-2}$	0.02
0.66	10^{-9}	$2.0 \cdot 10^5$	$2.3 \cdot 10^{-5}$	$4.00 \cdot 10^{-2}$	$4.0005 \cdot 10^{-2}$	0.01
0.68	10^{-8}	$1.0 \cdot 10^5$	$2.0 \cdot 10^{-4}$	$4.50 \cdot 10^{-2}$	$4.5140 \cdot 10^{-2}$	0.31
0.70	10^{-8}	$1.0 \cdot 10^5$	$1.8 \cdot 10^{-4}$	$5.00 \cdot 10^{-2}$	$5.0083 \cdot 10^{-2}$	0.17
0.72	10^{-8}	$1.0 \cdot 10^5$	$1.7 \cdot 10^{-4}$	$5.50 \cdot 10^{-2}$	$5.5050 \cdot 10^{-2}$	0.09
0.74	10^{-7}	$1.0 \cdot 10^5$	$1.5 \cdot 10^{-3}$	$6.00 \cdot 10^{-2}$	$6.0030 \cdot 10^{-2}$	0.05
0.76	10^{-7}	$1.0 \cdot 10^5$	$1.4 \cdot 10^{-3}$	$6.50 \cdot 10^{-2}$	$6.5018 \cdot 10^{-2}$	0.03
0.78	10^{-7}	$1.0 \cdot 10^5$	$1.3 \cdot 10^{-3}$	$7.00 \cdot 10^{-2}$	$7.0012 \cdot 10^{-2}$	0.02
0.80	10^{-6}	$5.0 \cdot 10^4$	$1.2 \cdot 10^{-2}$	$7.50 \cdot 10^{-2}$	$7.5601 \cdot 10^{-2}$	0.80

Figure 3: Parabolic velocity profiles between parallel rest plates, for $\tau = 0.80$, 1.00 and 1.60.



3.2 Entrance–region steady flow

If we consider wind-tunnel conditions at $x = 0$, i.e. an uniform velocity U in the inlet section, the velocity profile must become parabolic far downstream

$$u(y) = 6U \left(\frac{y}{H} - \frac{y^2}{H^2} \right) \quad (23)$$

An analytical approximate description of such experimental situation has been performed by Schlichting [9]. At the beginning, i.e. at small distances from the inlet section, the boundary layers will grow in the same way as along a flat plate at zero incidence. The resulting velocity profile will consist of two boundary-layer profiles on the two walls joined in the center by a line of constant velocity. Since the flow rate must be the same for every section, the decrease in the rate of flow near the walls which is due to friction must be compensated by a corresponding increase near the axis. Thus the boundary layer is formed under the influence of an accelerated external flow, as distinct from the case of the flat plate. At larger distances from the inlet section the two boundary layers gradually merge into each other, and finally the velocity profile is transformed asymptotically into the parabolic distribution (23). Schlichting estimated the inlet length as $l_E = 0.04 H Re$, where Re denotes the Reynolds number referred to the width of the channel, UH/ν . A comparison of results obtained with Lattice Gas Method to those computed by Schlichting was presented in [10].

The present LBM simulation was performed using a lattice with $N_w = 210$, therefore $H = 201\sqrt{3}/2 = 174.04$. The average velocity between plates was chosen $U = 0.01$ and the kinematic viscosity $\nu = 0.125$ (for $\tau = 1.0$). It results a small Reynolds number $Re = 13.925$ and $l_E = 97$. In this case, the Schlichting solution is not valid because the boundary layer approximation cannot be used and it is expected that the l_E value becomes larger. To overcome this situation, we choose $L = 200$.

In addition, in the boundary layer theory it is assumed that for incompressible flow the velocity profiles cannot have overshoots within the boundary layer but the results obtained with the Finite Element Method for entrance-region flow [11] do not confirm this assumption. Fig. 4 presents the velocity profile at four different distances from inlet section, obtained with LBM and FEM, respectively.

In order to verify if the domain length was large enough, the dimensionless velocity, u/U , variation versus x/H is presented in Fig.5. It can be seen that the curves reach asymptotically the values corresponding to the parabolic velocity profile (23).

Figure 4: Velocity profiles at different distances $x/H = 0.0718$ (a), 0.1436 (b), 0.2873 (c), 0.5746 (d) from the inlet section (solid curves – LBM results, dots – FEM solution).

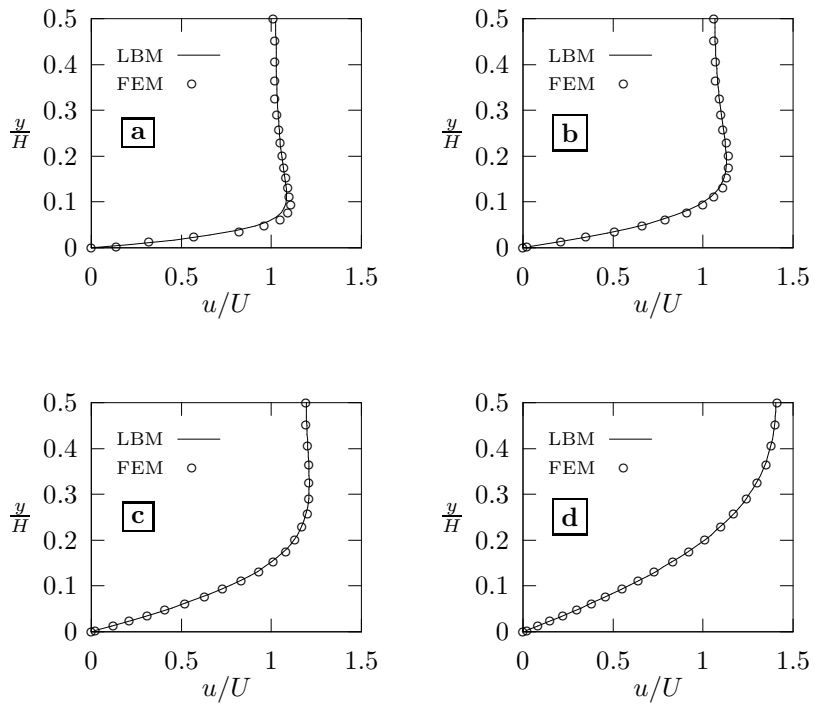
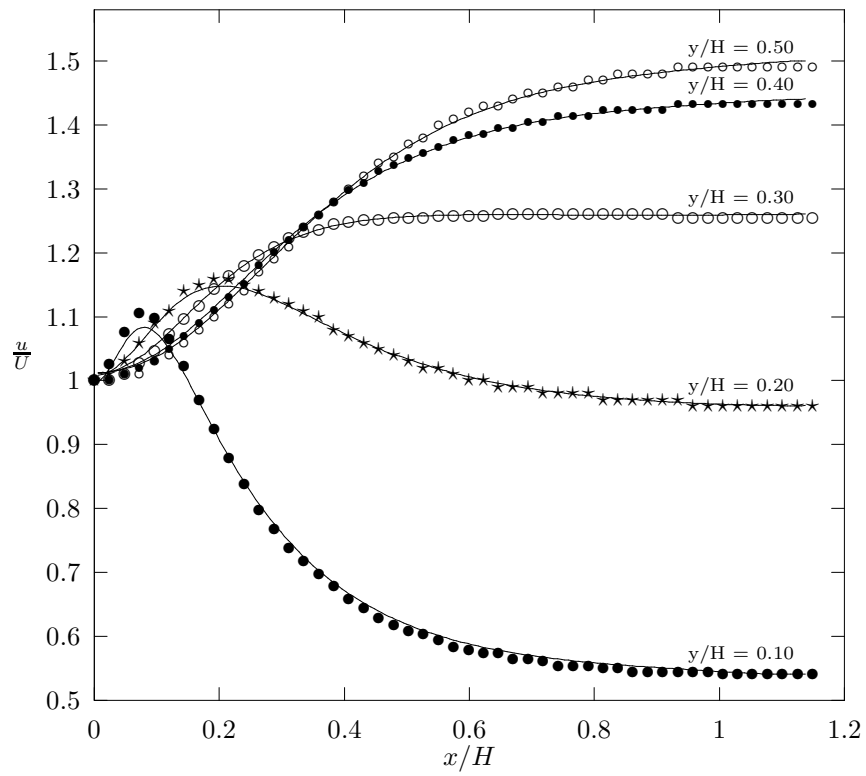


Figure 5: Velocity variation along the channel at different distances from the lower plate (solid lines – LBM results, dots – FEM solution).



3.3 Unsteady unidirectional flow

Let us consider an unidirectional flow for which the body force vanishes at the initial moment $t = 0$. The equation of motion is:

$$\frac{\partial u}{\partial t} = \nu \frac{\partial^2 u}{\partial y^2} \quad (24)$$

with the boundary and initial conditions:

$$\begin{aligned} u(0, t) = U(H, t) &= 0, \\ u(H/2, 0) &= U \end{aligned}$$

The solution is:

$$u(y, t) = U \exp\left(-\pi^2 \frac{\nu t}{H^2}\right) \sin\left(\pi \frac{y}{H}\right) \quad (25)$$

The free decay of the total fluid kinematic energy can be expressed as:

$$\frac{E_c(0)}{E_c(t)} = \exp\left(2\pi^2 \frac{\nu t}{H^2}\right) \quad (26)$$

and it can be used to calculate the kinematic viscosity from the slope of the $\ln [E_c(0)/E_c(t)] \leftrightarrow t$ line. Such lines are presented in Fig.6, the numerical results being obtained for a lattice with $N_w = 101$ and $N_l = 100$.

Table 2 presents the numerical and analytical values for ν , the relative difference being below 0.2%.

4 Time development of steady flow between parallel plates in relative motion

Suppose now that the fluid and the two parallel plates are initially at rest state. After the lower plate is suddenly brought to the steady velocity U in its own plane, while the upper one is still maintained at rest, the governing differential equation is (24) again, with the boundary and initial conditions

$$\begin{aligned} u(0, t) = U, \quad u(H, t) &= 0, \quad \text{for } t > 0 \\ u(y, 0) &= 0, \quad \text{for } 0 < y \leq H \end{aligned}$$

The velocity distribution is given by [8] :

$$u(y, t) = U \left(1 - \frac{y}{H}\right) \frac{2U}{\pi} \sum_{i=1}^{\infty} \frac{1}{i} \exp\left(-i^2 \pi^2 \frac{\nu t}{H^2}\right) \sin\left(i\pi \frac{y}{H}\right) \quad (27)$$

The LBM simulation was made for a lattice with $N_w = 101$ and $N_l = 100$. The distance between plates was now $H = 101 \sqrt{3}/2 - \sqrt{3}/4$. The term $\sqrt{3}/4$

Figure 6: Kinetic energy decay.

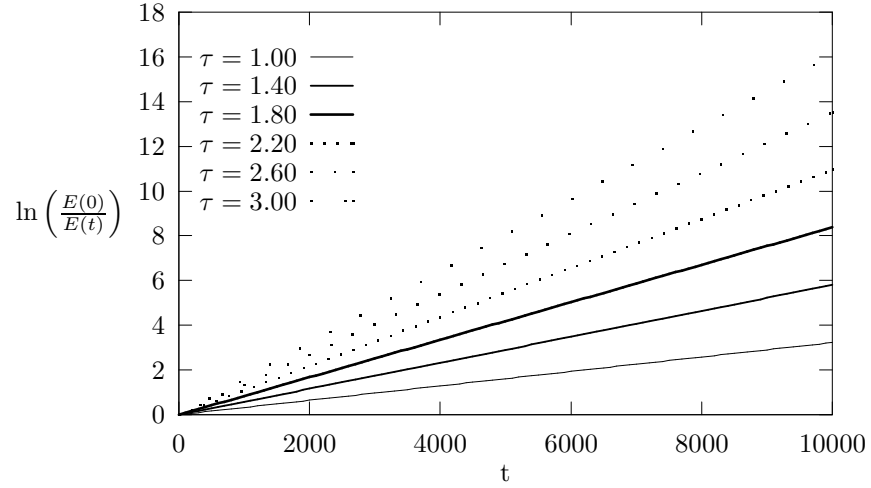
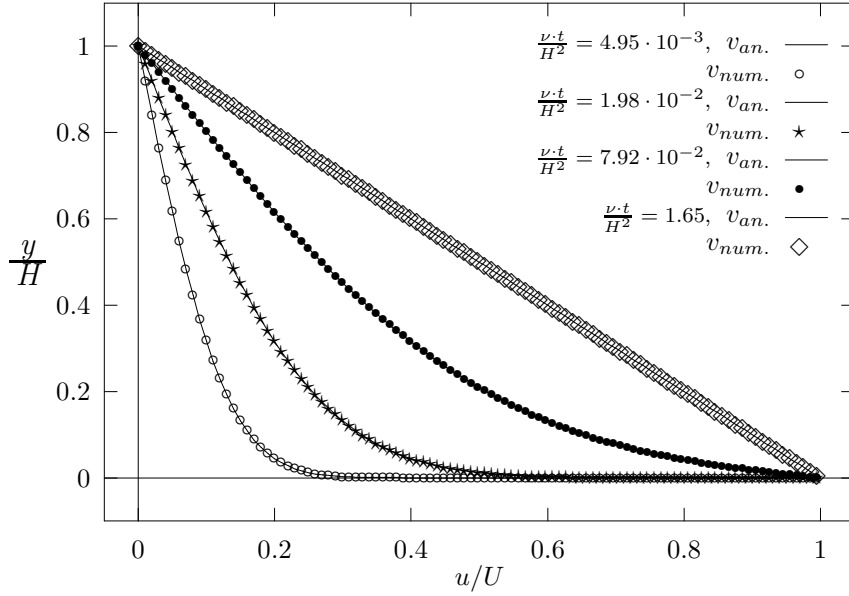


Table 2: Kinematic viscosities (ν_{an} from (14) and ν_{num} obtained from the kinetic energy decay) for $0.6 \leq \tau \leq 3.0$.

τ	ν_{an}	ν_{num}	ε_ν [%]
0.60	$2.50 \cdot 10^{-2}$	$2.50023 \cdot 10^{-2}$	0.0092
0.80	$7.50 \cdot 10^{-2}$	$7.50041 \cdot 10^{-2}$	0.0055
1.00	$1.25 \cdot 10^{-1}$	$1.25000 \cdot 10^{-1}$	0.0000
1.20	$1.75 \cdot 10^{-1}$	$1.74986 \cdot 10^{-1}$	0.0079
1.40	$2.25 \cdot 10^{-1}$	$2.24958 \cdot 10^{-1}$	0.0184
1.60	$2.75 \cdot 10^{-1}$	$2.74906 \cdot 10^{-1}$	0.0340
1.80	$3.25 \cdot 10^{-1}$	$3.24846 \cdot 10^{-1}$	0.0471
2.00	$3.75 \cdot 10^{-1}$	$3.74754 \cdot 10^{-1}$	0.0654
2.20	$4.25 \cdot 10^{-1}$	$4.24633 \cdot 10^{-1}$	0.0862
2.40	$4.75 \cdot 10^{-1}$	$4.74479 \cdot 10^{-1}$	0.1096
2.60	$5.25 \cdot 10^{-1}$	$5.24287 \cdot 10^{-1}$	0.1357
2.80	$5.75 \cdot 10^{-1}$	$5.74054 \cdot 10^{-1}$	0.1644
3.00	$6.25 \cdot 10^{-1}$	$6.23777 \cdot 10^{-1}$	0.1957

Figure 7: Development of velocity profile between parallel plates in relative motion without pressure gradient (dots – LBM results, solid lines – analytical solution, eq.27).



comes from the fact that we imposed the velocity $U = 0.01$ on the lower plate (there was no "bounce-back" condition there).

The time evolution of the velocity profile is represented in Fig. 7, at $t = 300, 1200, 4800$ and 10000 , the kinematic viscosity being $\nu = 0.125$.

An excellent concordance can be observed between the numerical and analytical results. The linear velocity profile corresponding to the steady Couette flow with no pressure gradient it is naturally obtained for $t \rightarrow \infty$.

5 Conclusions

A numerical approach to four kinds of flow between two parallel plates using the Lattice Boltzmann Method is presented. The number of lattice nodes was chosen in order to achieve an acceptable CPU time on Alfa DEC computers. The

numerical and analytical values of the kinematic viscosity were used to estimate the accuracy of the LBM simulations for both steady and unsteady unidirectional flows, the relative differences being found below one percent.

The zero velocity conditions on the rest channel walls were imposed by using "bounce-back" rules. The moving plate condition was achieved by forcing the the equilibrium distribution functions for the corresponding nodes in order to satisfy the imposed velocity.

Since the Schlichting approximate analytical solution for the entrance-region flow is inadequate at low Reynolds numbers, the comparison of the LBM results with a Finite Element Method solution was found to be appropriate.

Finally, we found an excellent agreement between the LBM computed time evolution of the velocity profiles and the analytical solutions of the Couette flow without pressure gradient.

Acknowledgments

The financial support of the Ministry of Education (contract 3012 / 1994) and of the Ministry of Research and Technology (contract 475 B / 1994) is gratefully acknowledged.

References

- [1] U. Frisch, B. Hasslacher and Y. Pomeau, *Phys. Rev. Lett.* **56** (1986) 1505.
- [2] U. Frisch, D. d'Humières, B. Hasslacher, P. Lallemand, Y. Pomeau and J.P. Rivet, *Complex Systems* **1** (1987) 649.
- [3] G. McNamara and G. Zanetti, *Phys.Rev.Lett.* **61** (1988) 2332.
- [4] F. Higuera and G. Zanetti, *Europhys.Lett.* **9** (1989) 663.
- [5] H. Chen, S. Chen and W. Matthaeus, *Phys.Rev. A* **45** (1992) 5339.
- [6] R.D. Kingdon, P. Schofield and L. White, *J.Phys. A* **25** (1992) 3559.
- [7] R. Cornubert, D. d'Humières and D. Levermore, *Physica D* **47** (1991) 241.
- [8] G.K. Batchelor, *An Introduction to Fluid Dynamics* (Cambridge Univ. Press, 1967) pp.180,191.
- [9] H. Schlichting, *Z.A.M.M.* **14** (1934) 368.
- [10] D. d'Humières and P. Lallemand, *C.R.Acad.Sc.Paris, Série II* **302** (1986) 983.
- [11] K.H. Huebner, *The Finite Element Method for Engineers* (John Wiley & Sons, New York, 1975) pp.341.